Micromechanical study of the interface properties in concrete repair systems

Mladena Lukovic, Branko Savija, Hua Dong, Erik Schlangen, Guang Ye

Journal of Advanced Concrete Technology, volume 12 (2014), pp. 320-339

Scientific paper

Micromechanical Study of the Interface Properties in Concrete Repair Systems

Mladena Luković[1*], Branko Šavija[2], Hua Dong[2], Erik Schlangen[3] and Guang Ye[4]

Received 7 April 2014, accepted 2 September 2014 doi:10.3151/jact.12.320

Abstract

Micromechanical interface properties in a concrete repair system determine the performance and reliability of a repaired structure. In order to characterize these properties, nanoindentation technique was applied. Three different repair material mixtures, based on Portland cement or partial replacement of Portland cement with blast furnace slag, were tested. Hardness and elastic modulus values obtained from the nanoindentation were used directly as input for simulated direct tension test. This way, the fracture behaviour of original microstructure, "mimicked" by Delft lattice model, is analysed. Backscattered electron (BSE) image analysis is utilized to estimate the average size of the interface zone which is distinguished as locally more porous area. This, together with simulation results, is further used for calculation of the interface stiffness. Simulation results enable prediction and better insight into fracture propagation and micromechanical response of the tested zone. They also indicate the ratio between interface and bulk material fracture properties when different types of repair materials are used. Load displacement diagrams of interface, old and new material can serve as an input for numerical modelling and understanding of fracture behaviour of the repair systems at the higher scale. Potentially, this approach may develop as a tool for verifying and engineering interface properties such that desired performance of the repaired structure is achieved.

1. Introduction

In order to make durable patch repair, it is important to understand the behaviour of a system made of two materials, and an interface layer between them. This interface is usually an inherently weak zone with a high probability of cracking when exposed to complex stress and strain state caused by incompatibility in properties between the old (concrete substrate) and new (repair) material. If the interface is very strong, however, high constraint levels might lead to cracking within the repair material or substrate. Consequently, interface properties at the contact between two materials will significantly affect the performance of the repaired structure and determine its potential failure pattern.

Still, knowledge regarding micromechanical properties of interfaces is lacking (Zhou 2010). This can be attributed to limitations of available test methods and difficulties in determining constitutive parameters at its size scale (microscale). The most commonly used criteria are various bond strength tests. A wide range of possible test set-ups have been developed and used for laboratory testing of the bond strength. Before dealing with the measurement of the bond strength, it is necessary to describe briefly the mechanism of failure. However, the location of failure is usually not well investigated, and these tests lack in providing information about what is actually happening in the failure zone (Beushausen and Alexander 2008). In addition, since failure propagation usually kinks into repair or substrate material, these tests generally provide information about the weakest link in the system, which is not always the interface itself. Therefore, a more fundamental approach is necessary, and it is important to investigate the properties of the interface at the microscale, similar to the way the interface between aggregate and cement paste (ITZ) is studied (Beushausen and Alexander 2008).

With the development of the nanoindentation technique, local micromechanical properties of the tested zones can be examined. From the indentation load and displacement measurements, hardness and E modulus of the indented volume are calculated. Indentation tests have been used by a number of researchers: Sakulich and Li (2011) measured mechanical properties of matrix-fibre interface, Zhu and Bartos (1997) used the microindentation method to measure the properties of the interfacial area in aged glass fibre reinforced cement, Wang *et al*. (2009) for interfacial area in steel fibre reinforced mortar and Xiao *et al*. (2013) were studying the interfacial transition zones in recycled aggregate concrete. Although the technique is very useful, this method has certain limitations, especially for heterogeneous materials such as cementitious ones. These tests are very sensitive to the surface preparation (Trtik *et al*. 2009;

[1]PhD Student, Delft University of Technology, Delft, the Netherlands.
[*]Corresponding author, *E-mail:* m.lukovic@tudelft.nl
[2]PhD Student, Delft University of Technology, Delft, the Netherlands.
[3]Professor, Delft University of Technology, Delft, the Netherlands.
[4]Associate Professor, Delft University of Technology, Delft, the Netherlands and Visiting Professor, Magnel Lab for Concrete Research, Department of Structural Engineering, Ghent University, Belgium.

Sakulich and Li 2011), as it directly influences the results and reliability of the obtained data. As a consequence, mechanical values obtained by various investigators have a wide variation range. In addition, due to the very heterogeneous structure of the interface on the microscale, with properties varying by wide margins, so far it has not been possible to convert microhardeness measurements into meaningful strength values (Maso 1996).

Still, this test is one of the few that involves only the interface zone itself, giving an indication of the distribution of local micromechanical properties inside the tested zone. In turn, this information may be used in micromechanical models that treat the interface as a highly heterogeneous zone which can be controlled, improved and modified in accordance with the designed performance of the system. In this study, therefore, the nanoindentation technique was applied in order to examine the interface properties in repair systems.

Portland cement paste, as a main constituent of cement-based repair materials and the main binding component at the contact zone between the two materials, was used as a repair material. By replacing Portland cement with various supplementary cementations materials, the chemical and physical properties of the material are altered and can be potentially improved. For example, the improvement of the interfacial microstructure in fibre reinforced cementitious materials was achieved by blending Portland cement with blast furnace slag (BFS) (Maso 1996). The content of calcium hydroxide (CH), one of the main products of Portland cement hydration, decreases with increasing BFS content (Zhou 2006). This suggests that CH is consumed by slag to form calcium silicate hydrates C-S-H-like reaction products, which densifies the cement paste. Also, large cementitious particles have loose packing at the contact zone between two materials and this results in higher porosity and lower cementitious content at the interface (wall effect). When BFS with finer particle size is used, improved particle packing at the interface can be achieved. Consequently, it is expected that when BFS is applied in a repair material, it may result in finer pore microstructure and lead to a more dense and uniform repaired interface zone.

However, the finer pore microstructure in BFS cement leads to larger autogenous shrinkage compared to Portland cement and, therefore, higher probability of cracking in the repair system (Van Cappellen 2009). Therefore, the beneficial influence of finer microstructure can be easily overweighed by higher stresses induced by autogenous shrinkage. The influence of BFS addition is expected to be very complex, and knowledge, especially in regard to the quantitative characterization of the influence of BFS on the interface properties, is limited. In this work, the influence of adding different amounts of BFS to the repair material on the micromechanical properties of the interface is therefore addressed and compared to properties of the Portland cement interface. Local elastic moduli and microhardness of different types of interfaces were quantified by nanoindentation tests. After this, the indented areas were imaged in ESEM (environmental scanning electron microscope) to capture the location of the indents, distance from the substrate and characterization of the phases that were indented.

Quantitative comparison of the local micromechanical properties is not sufficient for determination of the performance of the system. Value (what), fraction (how much) and distribution (where) of these properties, together with the state of the predominant stresses that the microstructure is exposed to, will determine the micromechanical response of the system. In order to predict this response, a numerical model was applied. The measured properties from the nanoindentation tests were directly used as input for numerical modelling. The stress-strain ratio for each indented microstructure, in a simulated direct tension test, is obtained. These nanoindentation tests combined with modelling, however, do not give the strength of the real interface at the contact area between two layers (i.e. the adhesion force between the two layers). It gives rather the strength of the interface layer which is, due to the wall effect, usually distinguished as a locally more porous area.

In order to calculate the interface stiffness, the size of the interface zone had to be estimated. Image analysis was used for this. For the very heterogeneous structure of the interface at the microscale, it is very difficult to provide a level of statistical confidence in the results. As illustrated by previous research (Diamond 2001), in which the interface between the cement paste and aggregates was studied, concrete microstructure in and around the interfaces is very complex and non-uniform. Instead, there are many local variations and groups of sites with similar properties ("clustering in properties") (Diamond 2001). Nevertheless, a tendency in porosity of the interface can be observed by applying image processing. Measured average thickness is used for the calculation of the interface stiffness.

As output from the simulated direct tension test, fracture properties of the interface can be compared to the fracture properties of the bulk matrix and mortar substrate. Using numerical testing, in this case, has two main advantages over experiments: first, the information obtained by nanoindentation can be directly used as input for "retesting" of the same specimen, now in a direct tension test; and second, boundary conditions, stability of the test set-up and uniform load distribution over the cross section are easily controlled in the model. In experiments, however, performing uniaxial test, even at mesoscale is difficult, while at microscale, is still impossible to achieve (Van Mier 2012). Fracture simulation results of tested microstructures and interface may further serve as input for higher-scale numerical modelling and understanding of global fracture behaviour of multi-layered systems.

2. Materials and methods

2.1 Materials

The substrate used in the study was a 5 year old mortar. The reason for using mortar (instead of concrete) was to minimize surface heterogeneity and specimen-to-specimen variation (Çopuroğlu and Schlangen 2008). The mortar was cast with Ordinary Portland Cement (OPC) CEM I 42.5 N, with a water-to-cement (w/c) ratio = 1:2, and somewhat higher cement-to-sand ratio = 1:1.65. Smaller mortar specimens were slowly cut with a diamond saw from bigger samples (**Fig. 1**). Specimens were cut in order to eliminate the interlocking effect and minimize the influence of surface roughness at this scale of testing, similar to how it is done with aggregate-cement paste interfaces (Struble and Mindess 1983). Old mortar cores were fixed in the centre of the moulds where the new material was later cast (**Fig. 1**). Before casting, the old mortar was placed for 24h in a chamber with 80% RH. This was done to enable hygral equilibrium and uniform moisture profile in all substrate specimens prior to casting of the new material.

OPC CEM I 42.5 N, and Blast Furnace Slag (BFS) were used as components for the repair material. Three mixtures for the repair material were designed. The water-to-binder (w/b) ratio of 0.4 was used in all cases. The composition details of all the mixtures are listed in **Table 1**.

Particle size distributions of the cementitious materials (OPC and BFS) are presented in **Fig. 2**. Finer BFS particles are expected to enable better packing at the interface compared to OPC.

After casting, specimens were cured for 28 days in sealed conditions at room temperature (20 ºC).

2.2 Sample preparation for nanoindentation

After 28 days, the samples were demoulded and cut with a diamond saw into small samples with a thickness of 8 mm. In order to stop the hydration, two methods were considered. Solvent exchange by isopropanol and freeze-drying showed to be the most effective for arresting hydration in young cement paste (Zhang and Scherer 2011). Due to the difference in the thermal expansion coefficients of young and old materials, instant cracking at the interface occurred immediately after placing the sample in the liquid nitrogen. Therefore, to stop hydration, isopropanol was used in this study. All samples were submerged five times and taken out for a period of one minute in order to enable faster water-solvent exchange. Afterwards, they were placed for 72 hours in isopropanol and subsequently taken out, at which point the solvent was removed by evaporation at ambient conditions.

In order to make the thickness of the specimens even and uniform, a thin sectioning machine was used for cutting and grinding the specimen. An object glass was glued on the sample and a block was cut with a diamond saw (**Fig. 3**). Afterwards, all samples were ground in the thin section machine in several passes. After grinding, each of the samples was polished with 6μm (5 min), 3μm (5 min), 1μm (5 min) and 0.25μm (25 min) diamond paste on a lapping table. After every step, an optical microscope was used to check the effectiveness of

Table 1 Mix proportion of the three specimens (weight percentage).

Mixture	Portland cement	Blast Furnace Slag	w/b ratio
CP	100	-	0.4
BFS1	80	20	0.4
BFS2	45.5	54.5	0.4

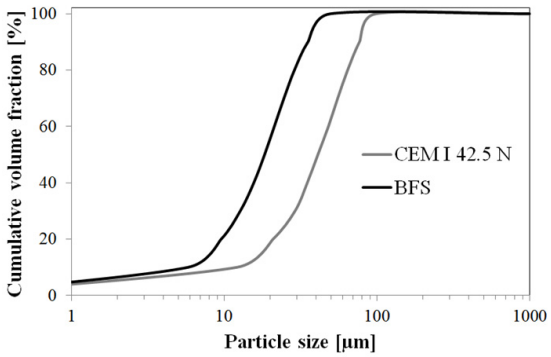

Fig. 2 Particle size distributions of cementitious materials.

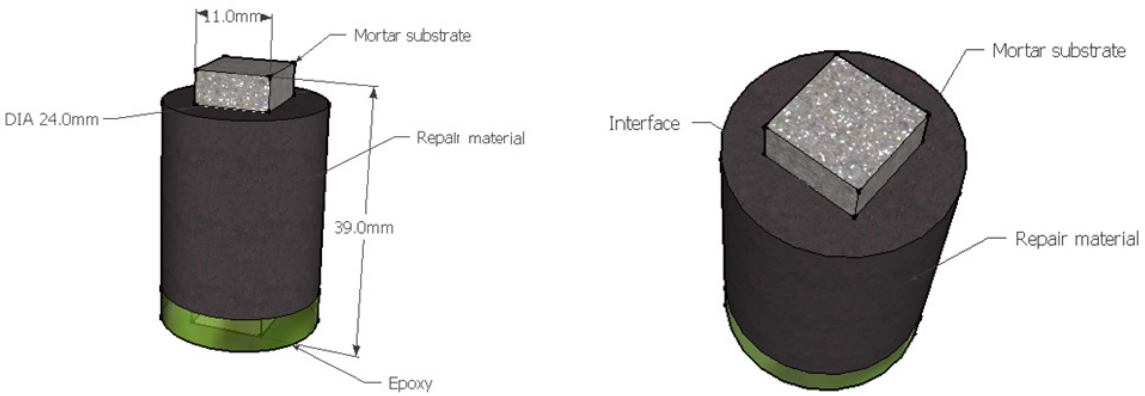

Fig. 1 Sample setup after casting repair material.

Fig. 3 Samples before grinding and polishing.

grinding and polishing. Finally, the samples were soaked into an ultrasonic bath to remove any residue from the surface. Samples were kept in a desiccator under vacuum until testing.

2.3 Nanoindentation and ESEM tests

Local mechanical properties of the tested points can be determined from the indentation load and displacement measurement (Oliver and Pharr 2004). Reduced elastic modulus, E_r (MPa) is the modulus that is computed directly from the measured load-displacement slope and calibrated contact area. However, as indenter deformation also contributes to the measured displacement, Young's modulus of the sample, E_s (MPa) is calculated from the reduced modulus, E_r (MPa) according to formula:

$$\frac{1}{E_r} = \frac{(1-\nu_s^2)}{E_s} + \frac{(1-\nu_i^2)}{E_i} \quad (1)$$

where, ν_s is the Poisson's ratio of the sample, ν_i is the Poisson's ratio of the diamond tip (0.07) and E_i is the Young's modulus of the diamond tip used for indenting (1141 GPa).

If P_{max} is the peak indentation load (mN), the hardness (H, GPa) has the definition as follows:

$$H = \frac{P_{max}}{A} \quad (2)$$

Agilent Nano Indenter G200 with a diamond Berkovich tip was used for nanoindentation tests. A quartz standard was indented before and after each test series to ensure accuracy. A series of indents were performed on a tightly spaced grid, with spacing of 7 μm in the direction perpendicular to the interface, and 14 μm in the direction parallel to the interface. The indentation depth was 700 nm. The Continuous Stiffness Method (CSM) developed by Oliver and Pharr (Oliver and Pharr 2004) was used. This method consists of superimposing a small oscillation on the primary loading signal and analysing the response of the system by means of a frequency-specific amplifier. As a consequence, it enables a continuous measure of contact stiffness (S, S=dP/dh) as a function of indentation depth (h) and not just at the point of initial unloading. Therefore, hardness and elastic, E modulus are obtained as a continuous function of surface penetration.

The average E modulus and hardness were determined in the displacement range between 500 and 650 nm depths. The indentation areas were taken randomly within the interface between the old mortar and new cement paste. Eight randomly chosen locations were tested in the case of the Portland cement interface (denoted as CP_I), seven in the case when 20% of cement replaced by BFS (denoted as BFS1_I) and 13 locations when more Portland cement was substituted by BFS (denoted as BFS2_I). Each location was tested with 200 indents. More locations in the BFS2 sample were tested because of the heterogeneity and somewhat lower workability of the mixture when a larger amount of cement was replaced by BFS. The number of sampling is the most important from the statistic point of view and representativeness of the results. Due to the high heterogeneity of cement paste and interface itself at the microscale, in this preliminary research, the minimum number of sampling for statistical confidence of results was not considered.

In order to eliminate the influence of additional parameters on the achieved properties, no superplastisizer was used in the repair material. All locations were chosen so that they include contact between the new and old cement paste (not the aggregate in the old mortar). Also, six randomly chosen locations (100 indents per location), far from the interface and in cement paste, were tested in the old material (**Fig. 4**). The same was done for the repair materials, i.e. Portland cement paste (denoted as CP_matrix) and BFS paste (denoted as BFS1_matrix and BFS2_matrix, respectively), where four and five locations, respectively, were tested with 100 indents per location.

After nanointentation testing, samples were examined using environmental scanning microscope (ESEM), in backscattered electron (BSE) mode. The instrument was operated at 20 kV accelerating voltage and at 10 mm working distance between the final condenser lens and the specimen. The spot size was 5.0 μm and the magni-

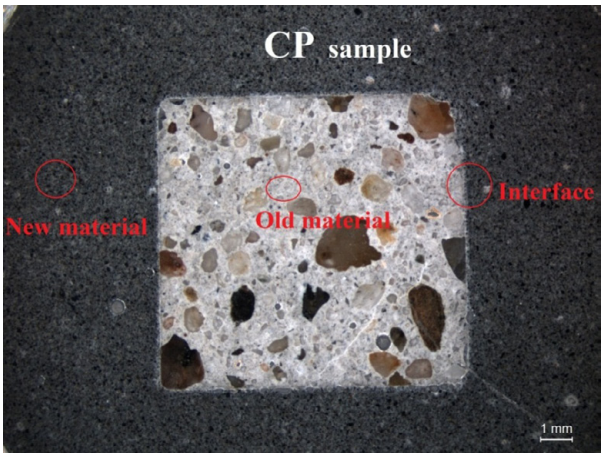

Fig. 4 Reflected light microphotograph of indentation spots. New material= Cement paste (CP), Old material = Substrate, 5 year old mortar.

fication was 500x. The vapour pressure inside the chamber was set to 1 Torr. All imaging was performed at low vacuum with vapour mode in order to reduce the probability of cracking in the specimens. The BSE images (25 per specimen) were used for image analysis as described later.

3. Experimental results and discussion

In the sample made with Portland cement paste (CP), eight locations were tested. The indented areas were imaged by BSE detector in ESEM (**Fig. 5 left**) and the location of the indents was correlated with the micromechanical properties to show their magnitude and distribution in the interface region. For the micromechanical properties, only the hardness values are presented (**Fig. 5 right**). Due to a high variety in obtained results and in order to put an emphasis on weak zones, the following procedure for visual representation is adopted: the data range was chosen so that it presents values up to 1.2 GPa in steps, while higher values are shown in one colour (light blue). This enables more insight into gradients and variations of lower properties which govern the fracture propagation at the interface. In the research carried by Hughes and Trtik (2004), mean hardness values for CSH inner and outer products were found to be around 0.88 GPa. This value can serve as a reference since lower properties than this are encountered when porosity and microcracking are present (dark blue, red and green colour). It has to be emphasized that it is not possible to clearly attribute values of physical properties to individual phases through this work, since the indentation depth (700nm) is large and, therefore, volume of different phases are present while indenting a certain location. However, the location of the indents and measured mechanical properties, around pores, unhydrated clinker particles and hydration products can be clearly linked to a corresponding microstructure in BSE image.

Samples with the addition of BFS (BFS1 and BFS2) were tested at seven and thirteen randomly chosen interface locations, respectively. The same procedure applied at the Portland cement interface was repeated for BFS_I samples. Some of the tested locations (7 per type of repair material) with the corresponding hardness values and legend are shown in **Fig. 6** (BFS1_I) and **Fig. 7** (BFS2_I). Due to space limitation, not all tested locations are presented.

The microcracking which is sometimes present in the testing zone (see image 5b) is due to exposure conditions in the ESEM, even though a low vacuum mode was used. The fast drying, incompatibility in the dimensional stability between new and old material, and probably locally lower interface properties are responsible for the cracking. Yet all tested locations were chosen such that prior to nanoindentation cracking was not present.

As can be seen from the presented results, properties of the old mortar seem to be uniform (hardness values higher than 0.9 GPa and indicated with blue and purple in **Figs. 5-7**). However, properties of the new material, around the interface (both for BFS_I and CP_I) differ in each of the tested locations. It seems that the weak area (red) can be regarded as the interface zone with lower properties at certain discrete locations, rather than an interface layer which propagates all the way parallel to the contact zone. Large amounts of CH present at the interface (**Figs. 5a, 5d, 5e**) locally increase mechanical properties at this zone. CH is observed in both CP_I and BFS_I specimens.

For the BFS2 sample, the interface shows much more microcracking compared to BFS1 and CP sample. In this case, cracking could be minimized through sample impregnation. However, as impregnation would influence the results of the mechanical testing (Hughes and Trtik 2004), the samples were not impregnated before testing.

In a previous study (Luković *et al*. 2013), it was shown that pure averaging and comparing of micromechanical properties at a certain location and distance from the contact zone does not provide any meaningful information. The very heterogeneous structure of the interface on the microscale contributes to high variations and a not so clear tendency around the interface. Also, these local micromechanical interface properties do not provide any information about the interface performance and its strength. They need to be linked in a structure where all the single local tests are assembled. By overlapping measured properties (E modulus and hardness) on a lattice mesh, tested microstructure is directly used as input for numerical modelling. Further on, in a simulated direct tension test, micromechanical response of the 'mimicked' microstructure can be estimated. This will enable assessment of the overall fracture performance of the interface zone at the microscale, with taking into consideration its intrinsic heterogeneity and real microstructure.

4. Modeling and discussion

4.1 Modelling details

Fracture processes of cement-based materials can be simulated with lattice models (Schlangen 1993). This approach was used both for mesoscale and microscale modelling of multi-phase materials (Schlangen *et al*. 2007; Landis and Bolander 2009). In this model, the material is schematized as a network of truss or beam elements connected at the ends. All individual elements have linear elastic behaviour. In each loading step, an element that exceeds limit stress or strain capacity is removed. The analysis procedure is then repeated until a pre-determined failure criterion is achieved. As this method addresses the physical processes that govern fracture behaviour, realistic crack patterns can be obtained. Furthermore, although each element has brittle behaviour, structural softening and ductile global behaviour can be simulated.

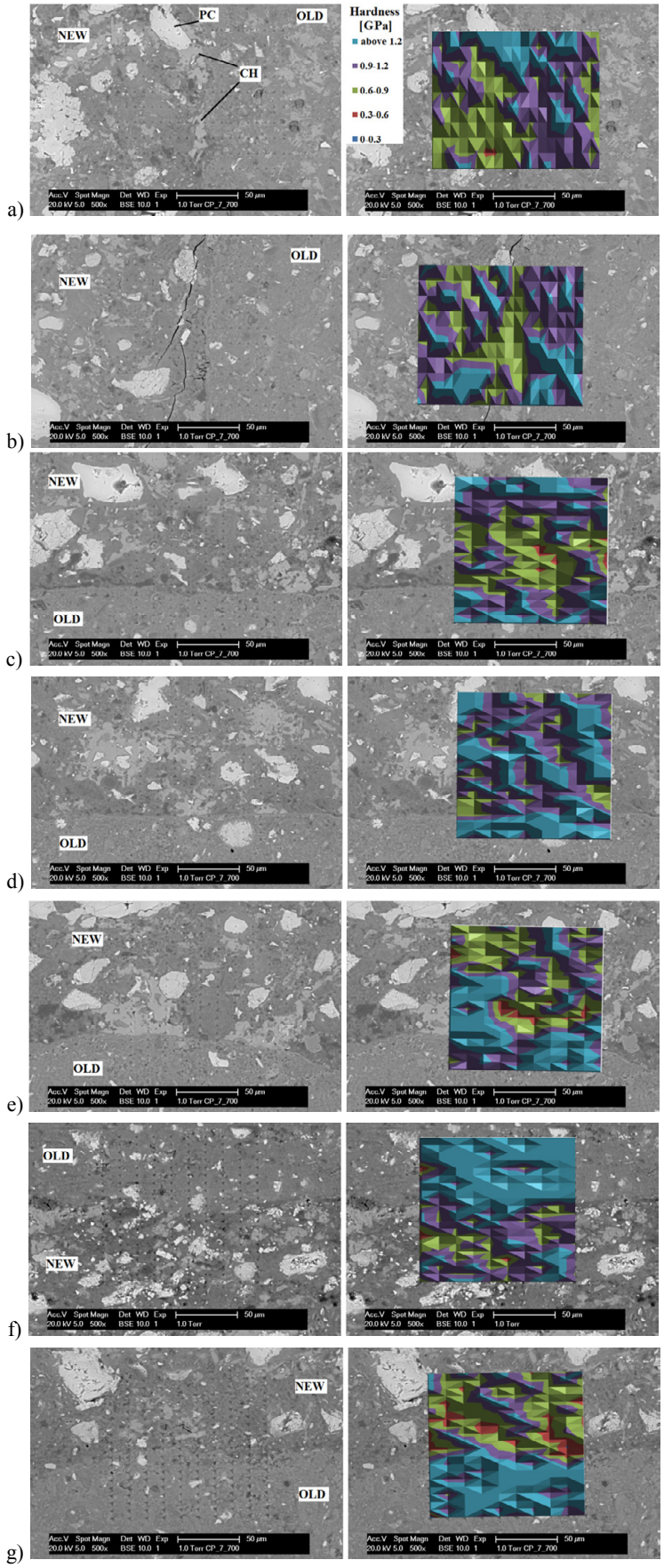

Fig. 5 Photomicrographs with corresponding hardness (H) values at location 1, 2, 3, 4, 5, 6, 7 (a, b, c, d, e, f, g) in CP_I.

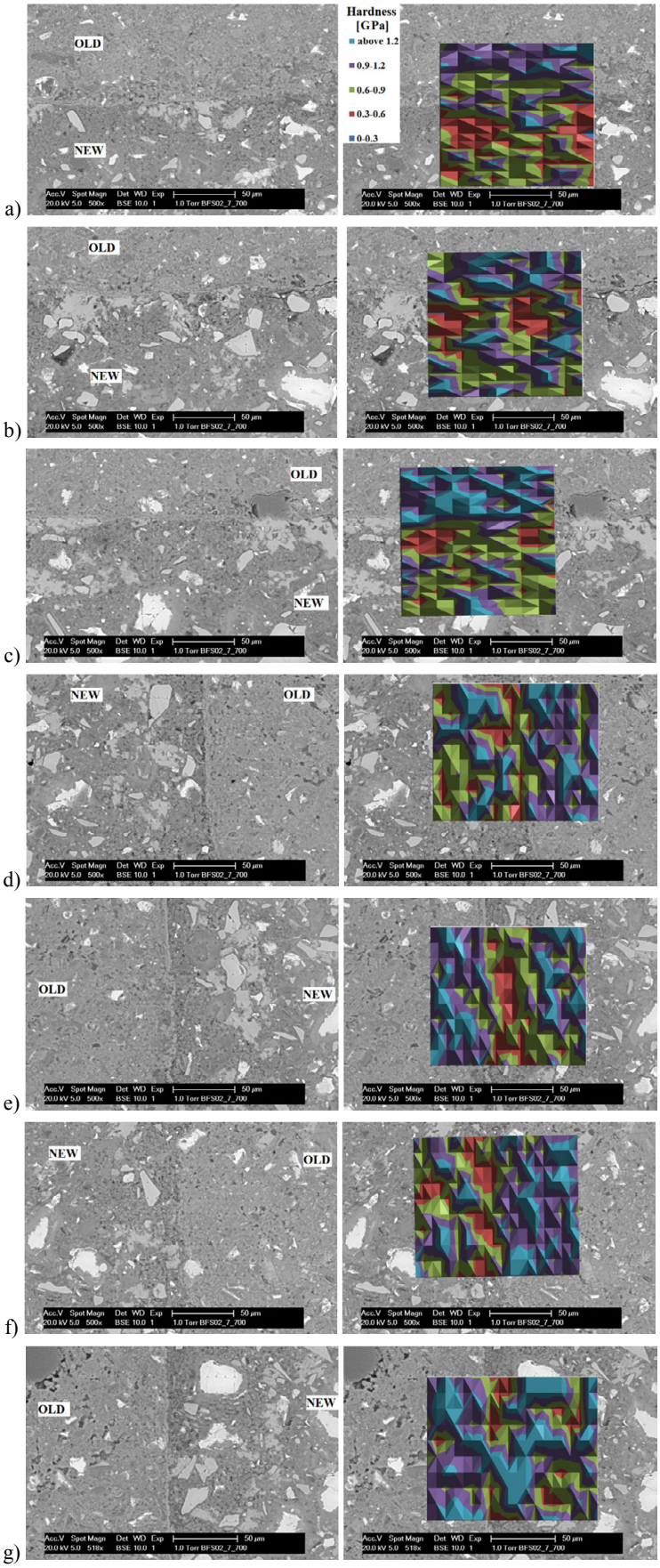

Fig. 6 Graphs with corresponding H values at the Location 1, 2, 3, 4, 5, 6, 7 (a, b, c, d, e, f, g) in BFS_1.

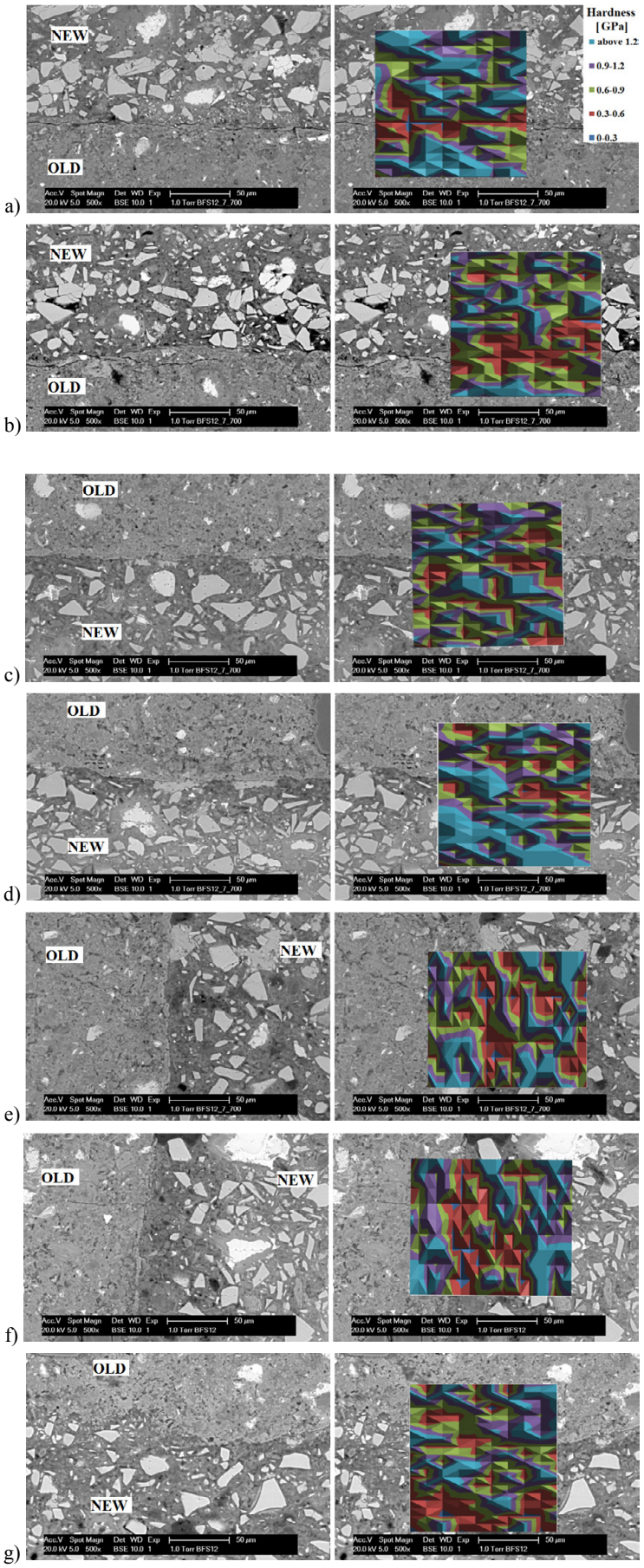

Fig. 7 Graphs with corresponding H values at the Location 1, 2, 3, 4, 5, 6, 7 (a, b, c, d, e, f, g) in BFS2_I.

In the 2D model used in this research, all beams have the same cross section. The procedure to generate the network is as follows:

- A square grid is chosen. In each square, a random location for a lattice node is generated. First the nodes are randomly positioned inside the sub cell of size s in a regular grid with size A (**Fig. 8**). The ratio s/A is defined as randomness of a lattice. Assigning certain randomness to the lattice mesh implements the heterogeneity of the material also through irregularities in the mesh geometry. When randomness is 0, node is located in the centre of cell and regular lattice mesh is generated. If the randomness is equal to 1, mesh is with the maximum degree of disorder. The choice of randomness affects the simulated fracture of materials, as different orientation of meshes can affect the crack shape (Schlangen and Garboczi 1997). A disadvantage of a regular mesh over irregular is that elements are preferentially orientated. Implementing randomness can reduce mesh dependency. However, if the randomness is very high, some of the beams can have very small lengths and then it might be difficult to distinguish the influence of geometry disorder from the influence of material texture. Therefore, in this work, in order to use the benefits of random mesh, but to avoid big variations in beam lengths, randomness of 0.5 was set. More information about the influence of randomness can be find elsewhere (Schlangen and Garboczi 1997; Lilliu and van Mier 2003; Qian 2012)
- The three nodes which are closest to each other are connected by beam elements. Each of the nodes has 3 degrees of freedom.
- Disorder in the material is additionally implemented by ascribing mechanical properties directly from the nanoindentation results. The Young moduli of elements are implemented from the measured elastic modulus values. The tensile strength ratio of each element is considered equal to the measured microhardness ratio (Qian 2012). In previous results (Luković *et al*. 2013), the hardness value was taken as an approximation for the compressive strength. However, the simulated tensile strength values appeared to be too high. One of the reasons for this is that, while indenting, the material is heavily confined under the indentation tip. When it fails, due to the limitations of the surrounding material under the indenting tip, the apparent strength is much higher than the actual strength, which leads to an overestimation of the simulated cement paste tensile strength. This is similar to results observed in (Zhang *et al*. 2011). They suggested that ratio of hardness and tensile strength is affected by the piled-up behaviours and ability of the tested material for shear deformation. Therefore, in materials with high ductility, the ratio between hardness and ultimate tensile strength is below 3, while the three-time relationship, widely used in literature, can be maintained in materials with medium shear deformability and plastic materials (different types of metals, alloys and metallic glasses). However, for ceramics and other brittle materials such as cement paste, the fracture strength and hardness showed a higher ratio. This is attributed to the limitations in shear deformability. In brittle materials, the shear deformation tends to be extremely difficult due to the material brittleness. As a consequence, the material is confined during indenting and this results in high measured hardness values. Therefore, the ratio between hardness and tensile strength of the material become much higher (it can vary from 28 to 183 for different types of ceramics (Zhang *et al*. 2011)). Since no published data was found defining this ratio in concrete or cement paste and in line with proposed values for ceramics, in the present simulations, a value 30 times lower than the hardness is taken as an approximation of the tensile strength, while compressive strength is considered to be 10 times higher than tensile strength.
- The beams which belong to each indented location are easily identified by overlapping tested properties on top of the lattice (**Fig. 8**). The elements that connect two cells which belong to neighbouring indented locations are ascribed with mean values from these two indents. As already mentioned, the indents located in big cracks or pores, were recorded as failed measurements. As cracks and pores do not contribute to global mechanical response, the elements that correspond to these indents were omitted from the mesh.
- Elements can fail either in tension or in compression, when stress exceeds strength. For the fracture criterion, only normal forces are considered to determine the stress in the beams.

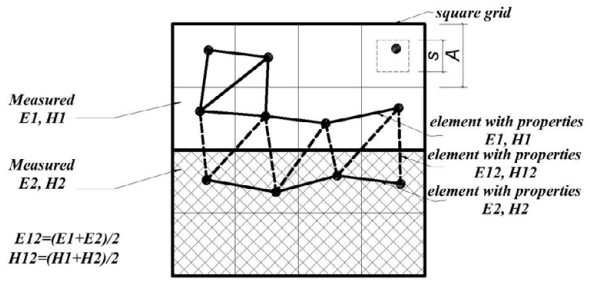

Fig. 8 Overlay procedure for lattice mesh.

4.2 Mesh sensitivity

The locations tested by nanoindentation were subjected to a simulated direct tension test. The interface specimens (BFS_I and CP_I) were loaded by applying uniform displacement at one edge, in a direction perpendicular to the interface (**Fig. 12b**). The movement and rotation of the opposite edge are restrained. Due to the node randomness and adopted mesh size, different ele-

ment alignments may cause some variations in the results for the simulated direct tension test. In order to estimate the influence of mesh size, 4 randomly generated meshes with the cell size of 3.5 µm and 1.75 µm (A in **Fig. 8**) and with the randomness value of 0.5 were generated for CP_I (Location 2). To make an overview of the lowest mechanical properties, the colour representation of the elements in the lattice mesh is the same as in **Figs 5, 6** and **7**. Damage patterns for the coarse and finer mesh are presented at the **Fig. 9**.

From **Fig. 9**, it is observed that for both coarse and fine mesh, the location of the crack remains consistent for all simulations. However, in the case of a coarse mesh, element orientation has more influence on the crack propagation. For the same cell size and adopted randomness value of 0.5, the fracture pattern still follows the same route, but can slightly deviate as a consequence of differences in alignment of the elements. In the case of a fine mesh, however, it seems that the influence of applied numerical modelling on the result deviation is lower. Furthermore, for the sample with cell size of 1.75 µm and randomness of 0.5 (i.e. fine mesh), the load displacement diagrams are compared and shown in **Fig. 10**. As can be seen from the presented diagrams, adopted randomness and mesh size do not have a significant influence on the load-displacement diagram in the simulated direct tension test. Therefore, cell size of 1.75 µm and randomness of 0.5 are used in all subsequent simulations.

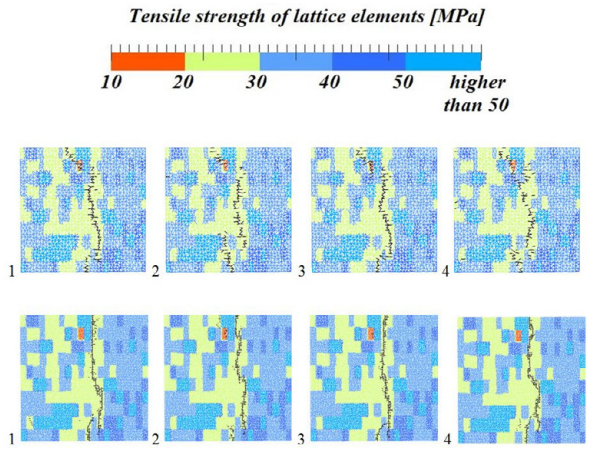

Fig. 9: Damage pattern in different meshes at the same number of damaged elements for the specimen CP_I, Location 2: Top=coarse mesh, Bottom=refined mesh (black - damaged elements).

4.3 Fracture parameters

One of the simulation results with crack development history is presented in **Fig. 11** (CP_I location 5). Snapshots from **Fig. 11 (a-f)** correspond to the points in the load-displacement curve (a-f) presented in **Fig. 12a**. The

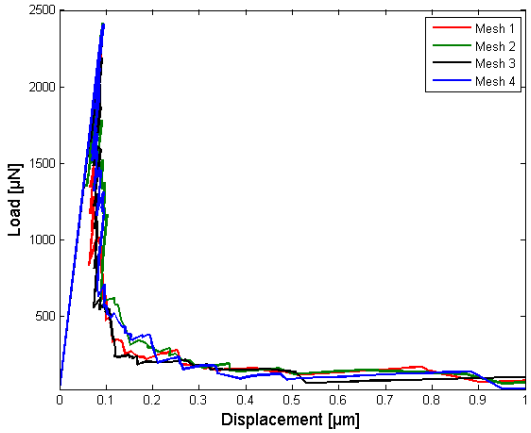

Fig. 10 Load-displacement diagrams for 4 different simulated meshes (cell size 1.75 µm).

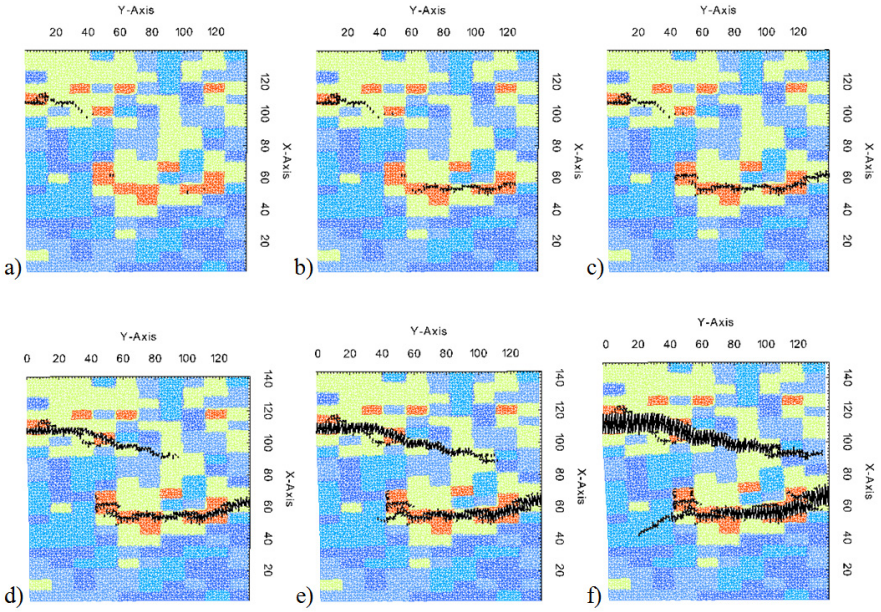

Fig. 11 Cracking history of the specimen in the simulated direct tension test for the specimen CP_I location 5 (deformation was scaled 10 times).

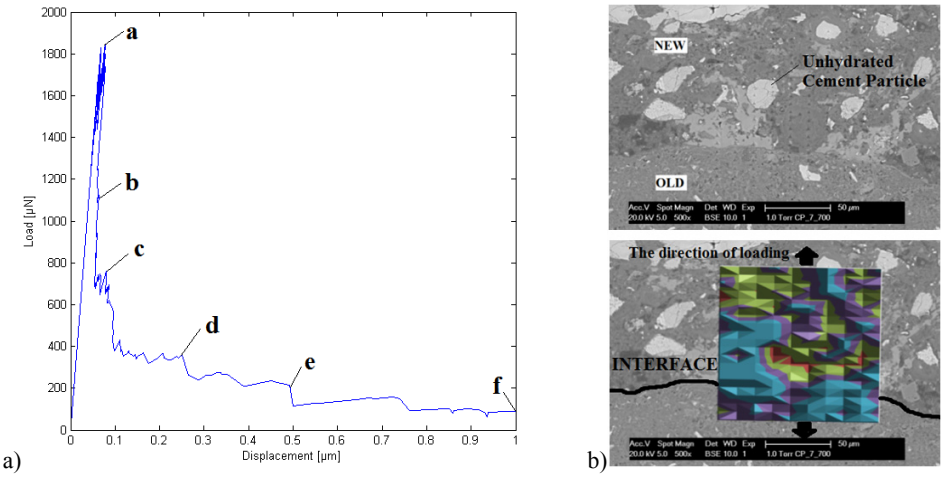

Fig. 12 a) Load-displacement diagram and b) the initial microstructure of the specimen CP_I location 5 (ESEM image with micromechanical properties).

first microcracking initiated approximately 50 μm from the contact zone between the two materials. This microcracking occurred before reaching the peak load (**Fig. 11a**). The crack stopped propagating in the vicinity of an unhydrated cement particle. Here, as the local material properties are higher, the crack was trapped and a new microcrack initiated at a different location. This new crack initiated close to the contact zone between two materials. Once the microcracking localized, stiffness of the tested "specimen" decreased, which resulted in softening post-peak region of the load-displacement curve (**Fig. 12a** and **11b**). Cracks nucleated and propagated further, finding their way through the neighbouring weak spots, located around unhydrated cement particles and the mortar substrate (**Figs. 11-c-e**). Two cracks deviated around an unhydrated cement particle (marked at **Fig. 12b,** top). This enabled some bridging between crack faces and disabled crack tips from connecting with each other and resulting in single crack localization (**Fig. 11f**).

The same procedure is repeated for all test locations, and stress displacement diagrams with crack history for all the test interfaces are obtained. If fracture occurred in the new material, up to 30 μm from the contact zone (interface thickness which was quantified in chapter 4.3.1 by image analysis), it was regarded as interface failure. In specimen CP_I location 5, although the first microcracking developed more than 30 μm from the contact zone, dominant cracking developed at the interface, and therefore it was also considered as interface failure. On the other hand, in the specimen CP_I location 4, although some microcracking was present at the interface, dominant failure occurred inside the repair material (more than 30μm from the interface) and was considered as a repair material failure (**Fig. 13b**). In specimen CP_I location 1 (see **Fig. 13a**), fracture occurred inside the substrate and therefore, was also not considered as interface failure. The peak load that was obtained, was used for the calculation of the mortar substrate strength. In the case of BFS1 specimens, all the failures occurred at the interface (i.e. **Fig. 13c**), while in case of BFS2, one failure occurred inside the mortar substrate (see **Fig. 13e**) and 2 in the repair material zone which is further than 30 μm from the interface (**Fig. 13f** and **13g**). Therefore, these failures were considered as bulk matrix failure, or failure of the repair material. It may also happen that the crack propagates exactly at the contact between the new and old material (see **Fig. 13d**). In the model, the intrinsic adhesion force directly at the contact between two materials is not explicitly considered, and therefore, this case of failure is not included in the simulation. This type of failure is also considered as interface failure.

For the CP_matrix and BFS_matrix (140 x 140 μm^2 tested area) and substrate mortar, the same procedure as for interface simulations is followed. In this case however, samples were loaded first in one direction and then in the perpendicular direction. This was done since neither the cement paste is an ideally isotropic homogenous material (Qian 2012), nor is the lattice perfectly isotropic (Lilliu *et al*. 1999), which means that loading direction somewhat influences the simulated stress-strain response. Further on, both results were taken when determining the average values of the response of the system.

From the simulation results, tensile strength, fracture energy and stiffness of the interface can be calculated. Fracture energy is calculated from the post peak part of a stress-crack opening diagram. It represents the area under the curve ($Gf = \int \sigma dw$, where σ is tensile stress and w is the crack width). Crack opening in lattice model is defined to be related to non-elastic deformation (i.e. crack opening is obtained by subtracting displacement due to elastic deformation from total displacement). In the present study, the fracture energy is calculated up to the total crack opening reaching 0.5 μm. Since in some samples instead of one crack, more cracks opened, fracture energy is calculated considering the whole tested "specimen". Therefore, higher fracture energy is calculated for the specimens where instead of

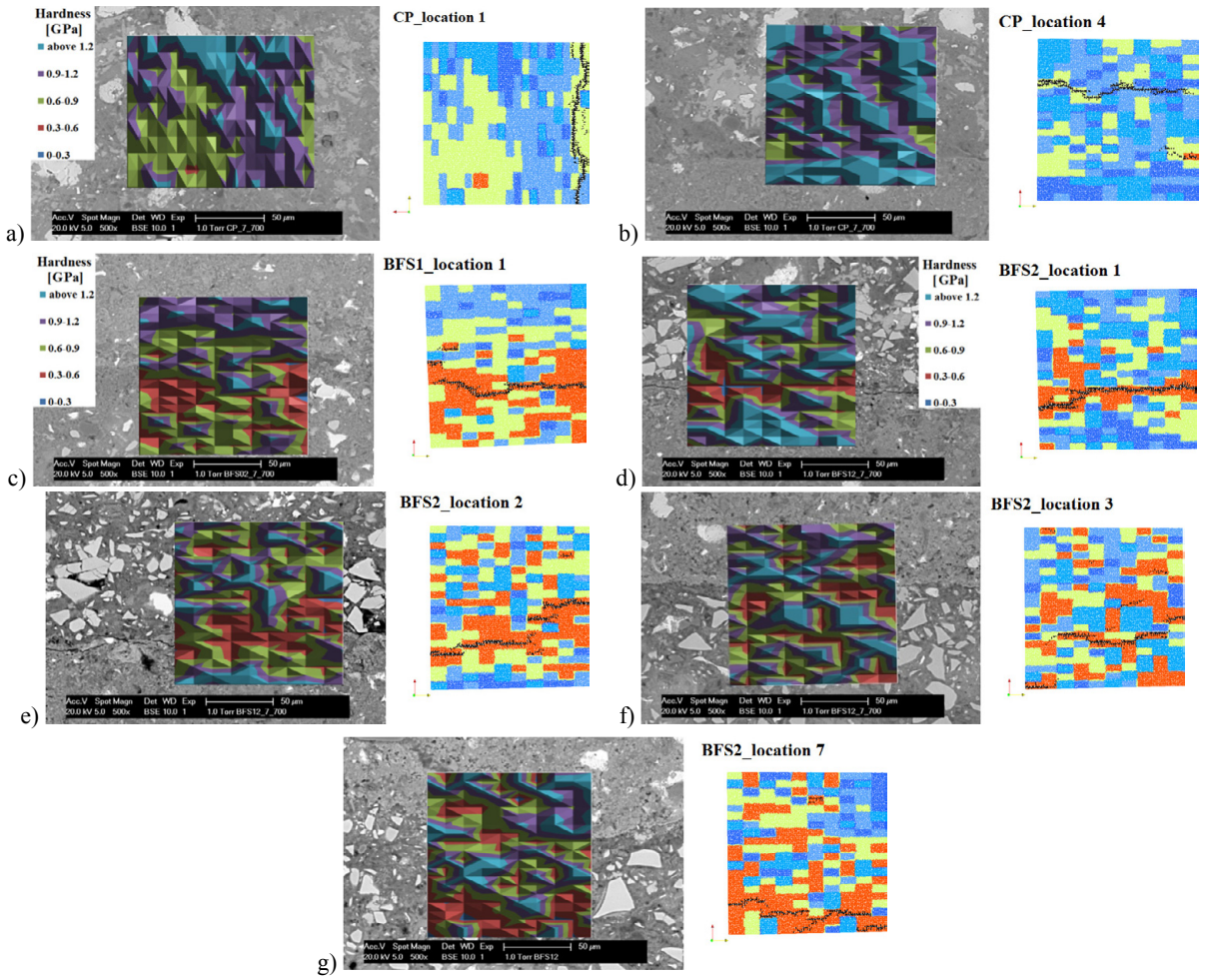

Fig. 13 Representative damage patterns in the specimens where interface, old or new material failed a) CP_location 1, b) CP_location 4, c) BFS1_location 1, d) BFS2_location 1, e) BFS2_location 2, f) BFS2_location 3, g) BFS2_location 7.

one crack, crack bridging is present (see CP_location 5, **Fig. 11**), and propagation of more cracks enabled more energy to be consumed until reaching the same total crack opening.

Elastic properties of the composite can be correctly "predicted" from lattice models, both for 2D and 3D analysis (Lilliu *et al*. 1999; Van Vliet 2000). As the calculated stiffness is influenced by the stiffness of the old material, interface stiffness and stiffness of the bulk new material, results obtained from the simulation were corrected to account for the areas of the old material, interface and bulk new material that were included in testing. The simplest way of calculating the stiffness of the composites is to revert to analytical models. Herein, a series model was used. The stiffness obtained in the simulation is therefore considered to be comprise of three springs combined in a series, representing mortar substrate, interface and bulk repair matrix. Therefore, the equation used to calculate interface stiffness is:

$$\frac{Aitz}{Eitz} = \frac{A}{E} - \frac{Aold}{Eold} - \frac{Anew}{Enew} \tag{3}$$

where A is the total area of a tested location (140 x 140 μm^2), $Aold$ is the area of old material, $Anew$ is the area of the new material, $Aitz$ is the area of the interface, E is Young's modulus obtained from simulation, $Eold$ and $Enew$ are the mean Young's moduli obtained from testing random spots in bulk old and new material, respectively, and $Eitz$ is interface Young's modulus. In order to obtain an average E modulus for the interface, the size of the interface zone needs to be estimated. As already mentioned, from the presented nanoindentation tests, the interface cannot be regarded as a layer with lower properties which propagates all the way parallel to the contact zone. However, an estimate about the width of this zone where locally lower properties are dominant is necessary for the calculation of the interface stiffness. This can be determined by averaging the nanoindentation results at a certain distance from the contact zone and comparing them to the bulk material properties (Lukovic *et al*. 2013). The very heterogeneous structure of the interface on this scale, however, contributes to high variations and a not so clear tendency around the contact zone. Also, there is a relatively small number of the tested locations and a limited area that these locations cover (140 x 140 μm^2). Another solution is apply-

ing an image analysis procedure, where the analysis might cover a larger area and therefore, enable more reliability in estimating the width of the interface zone. This method implies that the area fractions of unreacted cement, hydration products and capillary pores are segmented and compared. Although segmentation of the a digital image can never be error free, due to various reasons such as the finite-pixel size and overlapping of signal sampling volumes (Wong and Buenfeld 2009), these errors can be reduced if consistent thresholding rules are applied.

4.3.1 Image analysis

An image analysis procedure was used to quantify the average interface thickness which is needed to determine the interface stiffness. On the specimens prepared for the nanoindentation, the backscattered electron (BSE) imaging technique is applied according to the procedure explained in chapter 2. This enables estimation of the interface thickness which can be used later for the calculation of the interface stiffness. Images were taken randomly, around the contact zone between the new and old material. 25 images with 500x magnification were collected for CP_I and BFS1_I. In the BFS2_I sample, there was a limited number of images without cracks inside the specimens and therefore these specimens were not included in the image processing. The physical resolution of the image is 0.18 μm and the dimension is 1424x968 in pixel units.

First, in order to specify the contact zone between two materials, it was necessary to delineate the boundary of the substrate. Since computer automatic specification encounters difficulties (Diamond 2001), the boundary of the old material was specified manually (**Fig. 14d**). Further on, the image analysis is processed based on two algorithms: the concentric expansion method for the strip delineation (**Figs. 14e** and **14f**) and the overflow criterion for the pore segmentation (**Fig. 14b**) proposed by Wong *et al.* (2006). More details about these two methods can be found in (Gao *et al.* 2013a), where image analysis was used to examine the interface around aggregates in mortar specimens. The unreacted cement particles are segmented by selecting the minimum grey scale value between peaks for hydration products and the unreacted cement (**Fig. 14c**). Segmentation of BFS particles was not done, as the reflection intensities of hydration products under the BSE detector were quite similar to BFS particles. Area fractions of anhydrous cement particles and pores are analysed within the strips at a certain distance from the contact zone. For all the acquired images, stripes with varying widths of 5 and 10 μm were investigated (see **Figs. 14e** and **14f**).

Results obtained from the image analysis are presented in **Fig. 15**. As can be seen from the graph, there is a clear tendency that higher porosity and fewer unhydrated Portland cement particles are located close to the contact zone between two materials. The amount of un-

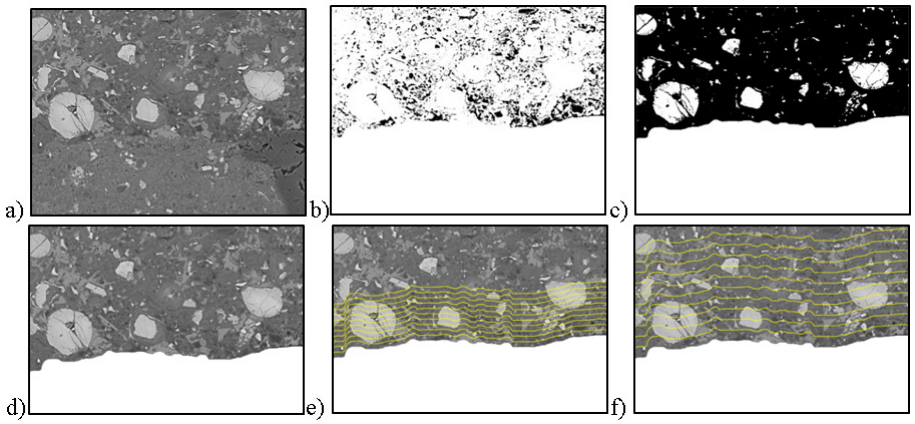

Fig. 14: Illustration of the image analysis procedure based on concentric expansion and overflow criterion: a) initial image, b) porosity around substrate, c) anhydrous Portland cement particles around substrate, d) initial image for strip delineation, e) strips with 5 μm thickness and f) strips with 10 μm thickness (the BSE image example is chosen from CP_I).

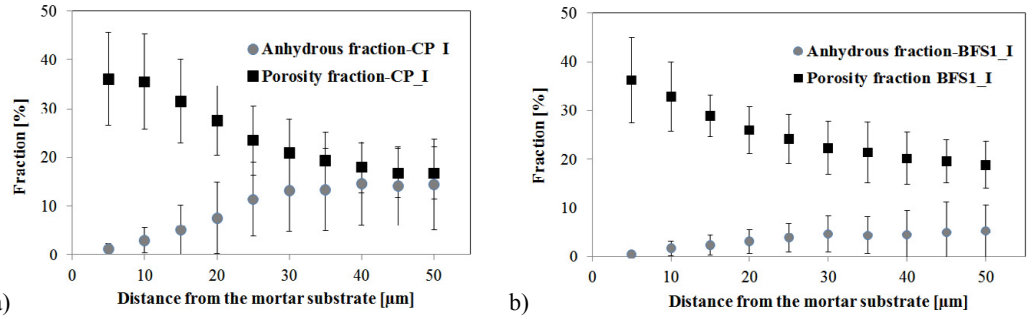

Fig. 15 Porosity and anhydrous fraction profiles based on ten 5 μm thick strips for a) CP_I and b) BFS1_I.

hydrated Portland cement particles in the case where 20% of the cement was replaced by BFS is lower due to their substitution with BFS particles. Also, since these particles are finer, the porosity profile for BFS shows a smoother decrease. However, the thickness of this interface zone, for both mixtures, seems to be similar. The same was observed in (Gao *et al*. 2013b) where, with the addition of BFS, porosity in the vicinity of the aggregate surface decreased, but the thickness of the interface zone did not. Therefore, for the different amounts BFS addition, the interface thickness (range in which these properties change) was the same. However, although showing the same tendency for both types of repair material used in this study, the thresholding value which should be adopted is not quite clear. Values between 30 and 40 μm seem reasonable for the interface thickness quantification and are, therefore, subjected to some bias.

In order to enable more precise estimation of the interface thickness, the degree of hydration for the CP_I is determined (**Fig. 16**). As the calculation of this parameter includes fractions of all the phases from the cement paste (unhydrated cement particles, hydration products and porosity), it might enable a more unbiased estimation of the width which can be further included for analysing the interface stiffness. Degree of hydration is determined only for CP_I, since in the case of BFS_I, greyscale values between unhydrated BFS and CH are too similar and therefore difficult to separate. However, based on previous discussions, the same thickness is expected in all types of interfaces, i.e. also when different amount of BFS are added to the repair material, and as such will be adopted in further studies.

The degree of hydration is calculated by dividing the fraction of the hydrated cement particles by the total sample fraction before hydration. As according to Powers' model (Powers and Brownyard 1947), the hydration products for Portland cement have a volume 2.1 times larger than that of the unhydrated cement particles, degree of hydration can be calculated as:

$$\alpha = \frac{Fhp/2.1}{Fhp/2.1 + Fuc} \tag{4}$$

where *Fhp* is the fraction of hydration products and *Fuc* is the fraction of unhydrated cement particles. The final degree of hydration which is obtained at the distance higher than 30 μm can be considered as bulk material degree of hydration and is around 0.71 with the standard deviation of 0.14. This is somewhat lower than 0.75 which was obtained by BSE image analysis done by Ye (2003) for the 28 days cement paste with w/c ratio of 0.4.

With the calculation of the degree of hydration in parallel stripes at a certain distance from the contact between the two materials, interface thickness seems to be easier to distinguish. Therefore, for all types of repair material investigated, interface thickness of 30 μm was adopted for the calculation of the interface stiffness.

4.4 Simulation results and discussion

Simulation results provide general insight about fracture properties of the interface, how the local micromechanical properties govern fracture propagation through the weak locations and how this determines the response of the system (**Figs 11** and **12**). Furthermore, simulation results obtained from the interface locations were compared to results obtained from the new material matrix and substrate matrix (See **Fig. 17**). Representative curves for different types of interfaces are presented in **Fig. 18**.

Results in **Fig. 17** indicate the ratio between interface and bulk repair material fracture properties. The simulated tensile strength that was obtained for 28-day cement paste with a w/c ratio of 0.4 corresponds well with values obtained by Qian (2012). Tensile strength of the interface is lower than the bulk matrix tensile strength. Also, the tensile strength of interfaces (BFS_I and CP_I) seem to follow the tendency of their matrixes, where the BFS_matrix (both for BFS1, bulk matrix and BFS2, bulk matrix) at the age of 28 days, due to slower hydration, shows lower properties than pure Portland cement paste. The same was observed in compressive tests done on mortar cubes where the different amount of PC was replaced by BFS (Menéndez *et al*. 2003). At

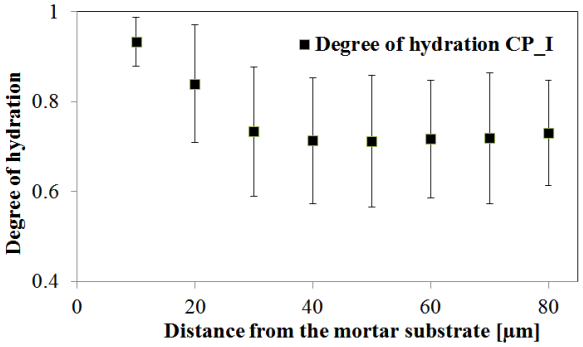

Fig. 16 Degree of hydration on 10μm thick strips for CP_I.

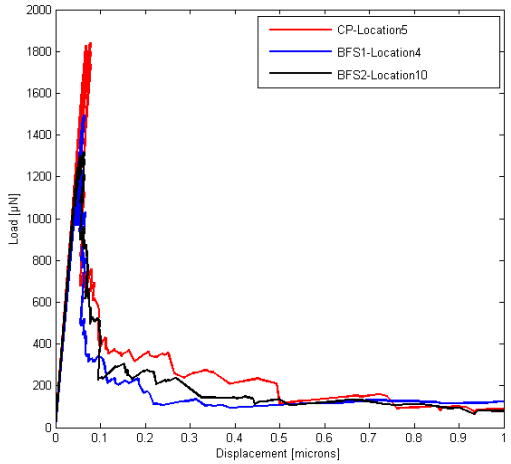

Fig. 18 Representative load-displacement curves for different interfaces.

the age of 28 days, addition levels of BFS (for 10%, 20% and 35%) reduced the compressive strength values by the ratio around 0.9 compared to the specimens with PC, while at the later age (90 days) addition of BFS resulted in higher compressive strength values. Therefore, it might be considered that the Pozzolanic reaction of BFS, by the age of 28 days, did not fully complete and therefore, through the diluting effect (increased w/c ratio) resulted in lower mechanical properties in blended mixtures compared to the pure Portland cement mixture.

Specimens with the addition of BFS (BFS_1 and BFS_2) showed similar tensile strengths, both in the interface zone and bulk matrix (**Fig. 17a**). However, if compared, the tensile strength of the BFS2 exhibits a higher standard deviation compared to the CP and BFS_1. The same holds for their interfaces (i.e. CP_I and BFS2_I). This can be attributed to the higher heterogeneity of the specimen which is a consequence of lower workability of the mixture when more Portland cement is replaced by BFS. The another reason might be that Portland cement triggers a faster hydration reaction and, if sufficiently present at the interface, enables more uniform properties. In the case where more Portland cement is replaced by BFS there is lower probability that Portland cement will be located in the interface, and therefore, more heterogeneity will be present depending on the packing. Therefore, although finer BFS particles enabled better packing at the interface, they did not enhance bonding properties at the age of 28 days. Slower hydration reaction of BFS particles compared to the Portland cement particles, reduced the amount of hydration products which would enhance the bonding by the age of 28 days. Therefore, the addition of BFS resulted in the reduction of tensile strength at the interface at the age of 28 days. In the case of CP and BFS_1 samples, results for the interface strength are based on the average value of 7 test locations while in the case of BFS_2, on 9 test locations which failed at the interface in the simulated direct tension tests. Although expecting that the tensile strength of cement paste inside the mortar would be more uniform due to its maturity, presence of aggregates and their distribution around the tested zones in the mortar probably increased the heterogeneity of microstructure and resulted in higher deviation in results. The tensile strength is lower compared to the 28 day CP_matrix (CP, bulk matrix), as a consequence of a higher w/c ratio of the mortar substrate.

Both for BFS and CP (matrix and interface), Young's (E) modulus shows a similar tendency as tensile strength (**Fig. 17b**). In the case where more Portland cement was substituted by BFS particles, the calculated stiffness of the specimens is reduced. The same was observed in the research done by Kurumisawa *et al.* (2010). They suggested that these reduced values are due to the different elastic behaviour of C-S-H in blended cement compared to that in Portland cement. Another reason may lay in the slower Pozzolanic reaction of BFS particles (Neville 1997; Zhou 2006). Due to

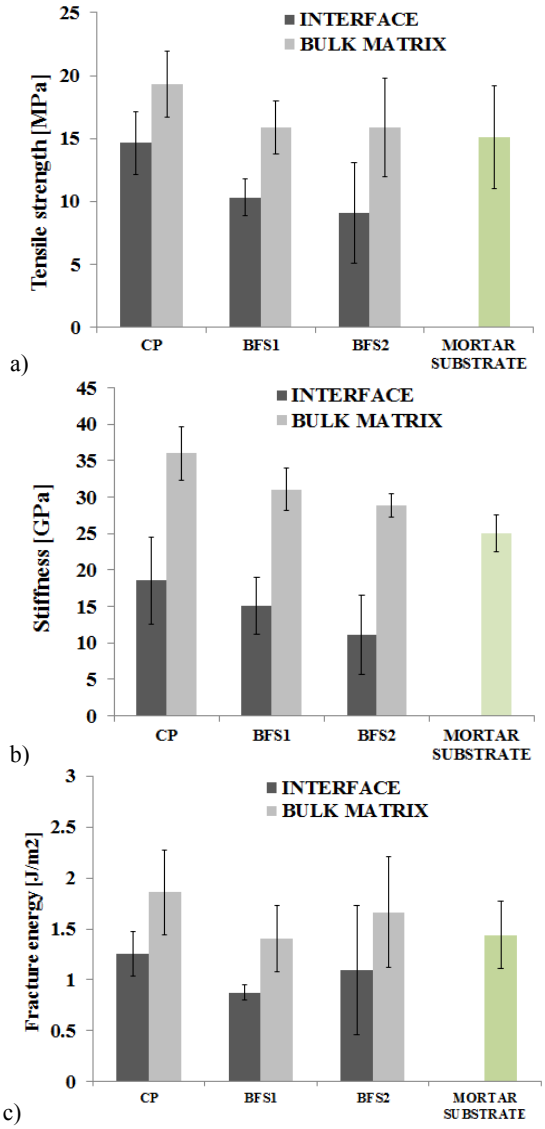

Fig. 17 Comparison of the interface and bulk material properties obtained from simulations: a) Tensile strength, b) Stiffness and c) Fracture energy.

the slower reaction, there is a dilution effect of the BFS particles, where the resultant w/c ratio is higher. Then, although contributing to the finer pore structure and lower effective porosity, total porosity in the blended mixture with the increasing BFS content is higher (Zhou 2006), and therefore the stiffness of the mixture is reduced.

For the matrix in the mortar substrate, although the degree of hydration is high, lower stiffness values are attributed to the higher w/c ratio. The value obtained for the mortar substrate matrix (around 25 GPa) is somewhat higher than the values obtained both numerically and experimentally by Constantinides and Ulm (2004). There, for the cement paste at the age of 5 months with a w/c ratio of 0.5, experimental (ultrasonic pulse velocity-UVP measurements) and numerical values of 22.8 GPa and 23.2 GPa were obtained.

For the repair matrix, with a w/c ratio of 0.4, at the age of 28 days, large amounts of unhydrated cement particles locally contribute to higher stiffness values. This stiffening role of the residual, unhydrated clinker on the properties of the hardened cement paste was noted in previous studies (Sorelli *et al*. 2008). Stiffness values obtained in the numerical simulation are somewhat higher than the stiffness values obtained by the UVP measurements at the age of 28 days. One of the reasons for this is the size effect. The measured stiffness is strongly dependent on the porosity. In nanoindentation tests, only porosity at smaller scales (<5 μm) is included. However, areas with bigger pores and air voids, which govern the behaviour in macroscopic tests are excluded as locations for testing were chosen such that they do not include big pores or air voids. The bigger the specimens, the more dominant the influence of big pores is and the lower the measured properties are. Larger volumes will have a larger probability of containing weak spots and consequently will fail at lower loads (Van Mier 2012). Similar observations were made by Velez *et al*. (2001), where nanoindentation measurements of the E modulus on pure Portland cement phases were compared to macroscopic scale measurement by the resonance frequencies technique. They observed consistency in results in microscopic and macroscopic scale measurements, where the porosity is the main influencing factor. When the elastic moduli obtained in the macroscopic scale tests were extrapolated to zero porosity, they were in a good agreement with the results obtained at the microscopic scale. The another important issue is that, although nanoindentation is measuring the micromechanical response of the indented volume, it considers information from only one slice of the tested area. Still, in macroscopic measurements of the E modulus, three-dimensional information is included. Pore connectivity and distribution of the air voids pores will play a dominant role in the response of the tested specimen and this is not taken into consideration in these microscopic tests.

Fracture energy of the interface is considered as a main parameter representing the interface fracture behaviour by many researchers (Kunieda *et al*. 2000; Martinola *et al*. 2001; Lau and Büyüköztürk 2010). Cement based materials exhibit a non-linear stress-strain relationship and microcracking before the peak stress. Afterwards, the crack localizes, which is followed by strain softening. The way this localization happens, followed by more microcracking, crack blunting, crack bridging, friction and crack arrest, will determine how much energy is absorbed during the fracture process. These mechanisms contribute to the tendency of the main crack to follow a tortuous route, consume more energy, enabling stable crack growth and avoiding brittle failure. The higher the fracture surface roughness (more tortuous and rugged), the higher the fracture toughness (Lange *et al*. 1993). Here, the fracture energy was calculated as the area under the softening part of the stress-displacement diagram up to a crack width reaching the size of 0.5 μm. From the presented results (**Fig. 17c**), it can be seen that the interface fracture energy is lower than that of the bulk material. This is due to lower peak strength but also lower amount of unhydrated cement and BFS particles due to the wall effect in the interface zone. The presence of unhydrated particles as locally stiff inclusions, will enhance crack bridging in the failure zone (see **Fig. 11**). With their presence, the crack does not propagate straight, but branches around these particles which consequently increase the amount of energy dissipation. Also, instead of a single crack tip, more microcracks develop, which consequently consumes more energy. The higher this energy consumption is, the more ductile the response of the system is, and higher fracture energy is spent on crack opening. When comparing CP_matrix to BFS1_matrix, it seems that the more homogenous the microstructure, the lower the fracture energy. Better packing of the particles in the BFS_matrix (both BFS_1, bulk matrix and BFS_2, bulk matrix in **Fig. 17c**) and finer particle size, results in a more uniform structure, more evenly distributed porosity, and therefore lower fracture energy. Instead of deviating and kinking in weak porous zones surrounding the bigger cement particles, cracks propagate fast, following more or less a straight route. Similar observations were made in (Nishikawa *et al*. 1995), where the fracture behaviour was investigated by compact tension from which the fracture energy of specimens was obtained. Samples with the addition of fine BFS resulted in decrease of fracture toughness compared to samples prepared only with Ordinary Portland cement. It was stated that large, unreacted cement particles brought a refraction in the crack or crack bridging which promoted resistance to crack propagation and enabled plastic behaviour after reaching maximum peak strength. On the other hand, finer BFS particles react with cement paste and water, becoming even smaller, leading to less tortuosity in crack bridging and less energy spent for crack development. Also, due to the dilution effect, the hydration of the remaining Portland cement particles is faster, which further reduces the size of unhydrated particles. The smaller the particle size, the fewer branching and grain bridging is achieved, and therefore less energy is consumed. The same is observed for the matrix in the mortar substrate. With the high w/c ratio and long curing age, the matrix reached a very high degree of hydration and relatively uniform microstructure, with a minimal amount of unhydrated particles which would cause crack branching.

If mean values for fracture energy are compared (**Fig. 17c**), different results can be observed for the BFS2 sample. High deviations found in these specimens are probably a consequence of the higher heterogeneity of the mixture, with lower workability during the casting procedure. Another reason is that these samples exhibited denser packing due to more BFS and its finer particle size. Further on, due to the slower Pozzolanic reac-

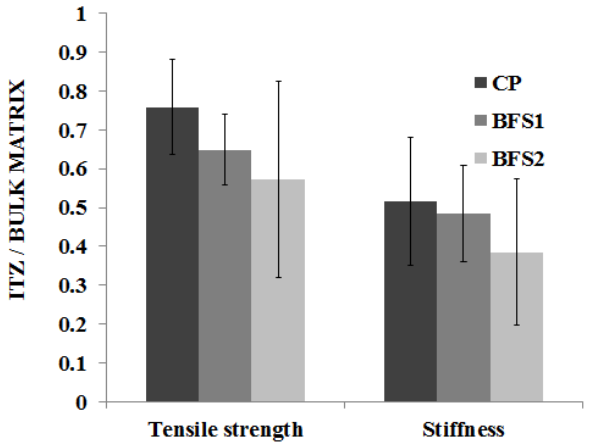

Fig. 19 Ratio between interface (ITZ properties) and bulk matrix properties for different type of repair material used.

tion and their dense packing, these particles do not reduce in size as fast as OPC. They still act as strong inclusions and enable crack tortuosity and branching, leading to a higher energy consumption during crack opening.

In **Fig. 19**, the ratios between the fracture properties of the interface and the corresponding bulk matrix (CP_I/CP_MATRIX, BFS1_I/BFS1_MATRIX and BFS2_I/BFS2_MATRIX) with calculated standard deviations are indicated. For the matrix properties, the mean value is taken. The highest ratio between interface and bulk matrix properties is obtained when only OPC is used. As the replacement level of OPC with BFS increases, the ratio decreases. This is reasonable as BFS particles, due to their finer particle size, tend to concentrate more in the interface. Therefore their local concentration in the interface will be higher than in the bulk matrix. With more BFS particles included, hydration of the paste is slowed down. Therefore, although finer packing is achieved, the ratio between the interface and bulk matrix strength when blended paste is used as a repair material is also lower compared to pure cement paste. The stiffness of the interface is around 50% lower than the stiffness of the bulk matrix and the ratio of the stiffness also reduces when the amount BFS added increases.

As can be seen, a large scatter of the results is present, especially when more BFS is used. This can be attributed to the intrinsic heterogeneity of tested samples and the test method itself. As the original microstructure was used, results encompassed inherent heterogeneity of material behaviour on multiple scales: nanoscale (hydrates distribution and gel porosity), microscale (capillary porosity, particle distribution, internal stress and strain state), mesoscale (influence of roughness, distance from the aggregate particles in the mortar substrate). On macroscale experimental testing, even more parameters have to be taken into account, which further complicates the quantification of the interface properties and leads to, unreliable predictions about the performance of the system.

Beside inherent heterogeneity, high variation of the results are also ascribed to the two dimensional representation of the microstructure. On top of the information that is included by indented volume (which is limited and determined by indentation depth), no information about pore connectivity, micro cracks, and distribution of the hydration products beneath this tested surface layer is obtained. More crack bridging and higher fracture energy, as well as a more uniform response of the system, would be expected if a three dimensional representation of the system would be possible.

Due to its heterogeneous nature, a significant number of interface locations should be tested before their statistical parameters can be determined. As previously stated, this was outside the scope of the current study.

Based on the presented results, one question that arises is whether the mean values for the interface are representative. Concrete and mortar microstructure in and around the interfaces are complicated and variable. The response of the system will be governed, not only by mean values, but more by the weakest properties, and therefore deviations of these properties should be also taken into account. Once localized, a crack will propagate and it will be difficult to stop it, especially in case of brittle cement based materials. For example, if BFS_1 and BFS_2 samples are compared, they have similar tensile properties but standard deviation in case of BFS_2 is much higher. Also prior to testing, finding an undamaged interface in case of BFS_2 was more difficult compared to BFS_1 sample. Furthermore, it is important to investigate how these variations influence the higher scale tests. As the interface is governing for the fracture response of the system (in mesoscale testing, i.e. aggregate matrix interface, or in macroscale testing, i.e. composite systems), mechanical models should encompass more information, such as probability and randomness of measured interface properties. This is especially important when the interface is the weakest link in the system.

5. Conclusions

The interface between old and new material in concrete repair systems is usually considered to be the weakest link of the system. So far, no significant attempts have been made to quantify the mechanical properties at its size scale. In the approach proposed herein, micromechanical tests are combined with numerical modelling to study mechanical properties and fracture behaviour of interfaces at the micro scale. Micromechanical properties of the interface and bulk material are measured by nanoindentation test and directly used as input in numerical modelling. Simulation testing, which mimics a bond strength setup and physical structure of the interface, might give insight into fracture processes at the interface. Based on results of this research, some conclusions can be drawn:

- The interface cannot be considered as a layer with uniformly lower properties close to the contact zone between two materials. Rather, it consists of local, discrete zones with low properties. However, these zones are usually initiation points for crack localization and together with local boundary conditions and phase distribution around this initial crack, they determine global fracture behaviour of multilayer materials.
- The ratio of tensile strength between the interface and bulk matrix at the age of 28 days for the cement based repair material is lower than 0.9. The ratio decreases as the addition of BFS increases. Although finer packing is achieved, BFS particles did not improve interface fracture properties at this age. This is attributed to the slower Pozzolanic reaction of the BFS particles compared to hydration of the Portland cement. Although finer packing is achieved, at the age of 28 days, the addition of BFS particles resulted in reduced strength.
- The ratio of stiffness between the interface and matrix is lower than 0.7 for all types of repair materials used. This is the consequence of the higher porosity of the interface, but also the lower amount of unhydrated particles which increase the local E modulus. With the addition of BFS, this ratio further decreases.
- Due to the size effect, stiffness values obtained in the simulated direct tension test are lower compared to (macroscopic) E modulus values obtained by ultrasonic pulse velocity measurement from the literature.
- Larger particles enable more crack bridging and therefore higher fracture energy. They act as obstacles, enabling locking of the cracks. When finer particles are used, a crack follows a straighter route, and less crack bridging is achieved. Therefore, fracture energy of pure cement paste is higher than with the addition of finely packed BFS.
- When ascribing mechanical properties to the interface in higher scale calculations, average properties probably should not be used. Instead, variations in E modulus and tensile strength should also be taken into account, as these lower tensile strength values and their randomness will govern the response of the whole system.

Numerical modelling combined with experimental testing can potentially bridge the gap between local material properties inside the system and its structural behaviour at the microscale. Furthermore, it is a promising attempt to quantify, at least in the comparative sense, the relationship between fracture properties of the interface and bulk mechanical properties of the material.

The important question that arises here is, once the interface properties are quantified, whether it is representative to use their mean values. The locations that were tested were chosen to be without cracks and defects. The interface is not homogenous and measurements specifically reflecting the local variations are important for a proper representation and realistic model. Local variations are a result of complicated physical and chemical processes which are taking place due to the interaction between two materials. These processes are still not fully understood. Therefore, at this scale it is still not possible to explain it by using simplified models, nor is a wide range of experiments available for their testing. One approach for studying the interface properties is inverse modelling, but in order to determine both interface properties and properties between different phases in cement based materials, fracture tests at the microscale need to be conducted. So far, this was not possible. Another approach is experimental testing in available tests (nanoindentation) in order to quantify the local properties and assemble these measured properties by applying modelling procedure that was previously described. In this way, realistic material representation is included and used as the input. Then simulated properties, both for the bulk material and interface zone can be compared. It has to be highlighted that this approach, however, does not cover the adhesion force between the two layers. It gives rather the strength of the interface layer which is, due to the wall effect, usually distinguished as a locally more porous area. Results obtained from simulated experiments based on realistic material representation could be used as input for higher scale simulation and testing which is possible to perform and verify by experimental results. Determining and understanding the interface properties at its size scale is essential and will help to explain observations from meso/macroscale fracture tests. Furthermore, the used approach might enable better understanding of the complex fracture processes of multilayer systems, which is almost always dictated by fracture properties of the their interface.

Acknowledgements

Financial support by the Dutch Technology Foundation (STW) for the project 10981-"Durable Repair and Radical Protection of Concrete Structures in View of Sustainable Construction" is gratefully acknowledged.

References

Beushausen, H. and Alexander, M., (2008). "Bond strength development between concretes of different ages." *Magazine of Concrete Research*, 60(1), 65-74.

Constantinides, G. and Ulm, F. J., (2004). "The effect of two types of CSH on the elasticity of cement-based materials: Results from nanoindentation and micromechanical modeling." *Cement and Concrete Research,* 34(1), 67-80.

Çopuroğlu, O. and Schlangen, E., (2008). "Modeling of frost salt scaling." *Cement and Concrete Research,* 38(1), 27-39.

Diamond, S., (2001). "Considerations in image analysis as applied to investigations of the ITZ in concrete." *Cement and Concrete Composites,* 23(2), 171-178.

Gao, Y., De Schutter, G., Ye, G., Huang, H., Tan, Z., and Wu, K., (2013a). "Porosity characterization of ITZ in

cementitious composites: Concentric expansion and overflow criterion." *Construction and Building Materials,* 38, 1051-1057.

Gao, Y., De Schutter, G., Ye, G., Yu, Z., Tan, Z., and Wu, K. ,(2013b). "A microscopic study on ternary blended cement based composites." *Construction and Building Materials,* 46, 28-38.

Hughes, J. J. and Trtik, P., (2004). "Micro-mechanical properties of cement paste measured by depth-sensing nanoindentation: a preliminary correlation of physical properties with phase type." *Materials Characterization,* 53(2), 223-231.

Kunieda, M., Kurihara, N., Uchida, Y., and Rokugo, K., (2000). "Application of tension softening diagrams to evaluation of bond properties at concrete interfaces." *Engineering Fracture Mechanics,* 65(2), 299-315.

Kurumisawa, K., Nawa, T., and Hirukawa, Y., (2010). "Micro elastic modulus of blended cement pastes" In: Takanabe *et al*. Eds. *Creep, Shrinkage and Durability Mechanics of Concrete and Concrete Structures*, *Proceedings of the CONCREEP 8 conference held in Ise-Shima, Japan, 30 September-2 October 2008*, CRC Press.

Landis, E. and Bolander, J. E., (2009). "Explicit representation of physical processes in concrete fracture." *Journal of Physics D: Applied Physics,* 42(21), 214002.

Lange, D. A., Jennings, H. M., and Shah, S. P., (1993). "Relationship between fracture surface roughness and fracture behavior of cement paste and mortar." *Journal of the American Ceramic Society,* 76(3), 589-597.

Lau, D. and Büyüköztürk, O., (2010). "Fracture characterization of concrete/epoxy interface affected by moisture." *Mechanics of Materials,* 42(12), 1031-1042.

Lilliu, G., van Mier, J. G. M, van Vliet, M. R. A., (1999). "Numerical characterization of the elastic properties of heterogeneous materials with a 3D lattice model." *International Series on Computational Engineernig*, 515-524.

Lilliu, G. and van Mier, J. G. M., (2003). "3D lattice type fracture model for concrete." *Engineering Fracture Mechanics*, 70(7), 927-941.

Luković, M., Šavija, B., Schlangen, E., and Ye, G., (2013). "Micromechanical study of the interface properties of concrete repair systems". In: Li, Z.J., *et al*. Eds. *Proceedings of the Seventh International Conference on Concrete under Severe Conditions-Environment and Loading (CONSEC13). Nanjing, China*

Lukoviić, M., Schlangen, E., Ye, G., and Šavija, B., (2013). "Impact of surface roughness on the debonding mechanism in concrete repairs." In. van Mier, J. G. M. *et al* Eds. *Proceedings of the 8th International Conference on Fracture Mechanics of Concrete and Concrete Structures (FraMCoS-8), Toledo, Spain.*

Martinola, G., Sadouki, H., and Wittmann, F. H., (2001). "Numerical Model for Minimizing the Risk of Damage in a Repair System." *Journal of Materials in Civil Engineering,* 13(2), 121-129.

Maso, J., Ed., (1996). "*Interfacial transition zone in concrete."* RILEM Report 11, E&FN Spon.

Menéndez, G., Bonavetti, V., and Irassar, E. F., (2003). "Strength development of ternary blended cement with limestone filler and blast-furnace slag." *Cement and Concrete Composites,* 25(1), 61-67.

Neville, A. M., (1997). "*Properties of concrete*". 4th and final ed. Harlow, UK: Pearson Education Limited.

Nishikawa, T., Takatsu, M., and Daimon, M., (1995). "Fracture behavior of hardened cement paste incorporating mineral additions." *Cement and Concrete Research,* 25(6), 1218-1224.

Oliver, W. C. and Pharr, G. M., (2004). "Measurement of hardness and elastic modulus by instrumented indentation: Advances in understanding and refinements to methodology." *Journal of Materials Research,* 19(1), 3-20.

Powers, T. and Brownyard T., (1947). "Studies of the physical properties of hardened portland cement paste." *ACI Journal Proceedings, ACI*.

Qian, Z., (2012). "*Multiscale Modeling of Fracture Processes in Cementitious Material*", PhD thesis. Delft University of Technology, The Netherlands.

Sakulich, A. R. and Li, V. C., (2011). "Nanoscale characterization of engineered cementitious composites (ECC)." *Cement and Concrete Research,* 41(2), 169-175.

Schlangen, E., (1993). "*Experimental and numerical analysis of fracture processes in concrete.*" PhD thesis, Delft University of Technology, The Netherlands.

Schlangen, E. and Garboczi, E. (1997). "Fracture simulations of concrete using lattice models: computational aspects." *Engineering Fracture Mechanics*, 57(2), 319-332.

Schlangen, E., Koenders, E. A. B., and van Breugel, K., (2007). "Influence of internal dilation on the fracture behaviour of multi-phase materials." *Engineering Fracture Mechanics,* 74(1), 18-33.

Sorelli, L., Constantinides, G., Ulm, F. J., and Toutlemonde, F., (2008). "The nano-mechanical signature of ultra high performance concrete by statistical nanoindentation techniques." *Cement and Concrete Research,* 38(12), 1447-1456.

Struble, L. and Mindess, S., (1983). "Morphology of the cement-aggregate bond." *International Journal of Cement Composites and Lightweight Concrete,* **5**(2), 79-86.

Trtik, P., Munch, B., and Lura, P., (2009). "A critical examination of statistical nanoindentation on model materials and hardened cement pastes based on virtual experiments." *Cement and Concrete Composites,* 31(10), 705-714.

Van Cappellen, J., (2009). "*Autogenous and drying*

shrinkage." MSc thesis, Delft University of Technology, The Netherlands.

Van Mier, J. G. M., (2012). "*Concrete fracture: A multi-scale approach"*, CRC Press: Boca Raton

Van Vliet, M. R. A., (2000). "*Size effect in tensile fracture of concrete and rock."* PhD thesis, Delft University of Technology, The Netherlands.

Velez, K., Maximilien, S., Damidot, D., Fantozzi, G., and Sorrentino, F., (2001). "Determination by nanoindentation of elastic modulus and hardness of pure constituents of Portland cement clinker." *Cement and Concrete Research,* 31(4), 555-561.

Wang, X. H., Jacobsen, S., He, J. Y., Zhang, Z. L., Lee, S. F., and Lein, H. L., (2009). "Application of nanoindentation testing to study of the interfacial transition zone in steel fiber reinforced mortar." *Cement and Concrete Research,* 39(8), 701-715.

Wong, H. and Buenfeld, N. R., (2009). "Determining the water–cement ratio, cement content, water content and degree of hydration of hardened cement paste: Method development and validation on paste samples." *Cement and Concrete Research,* 39(10), 957-965.

Wong, H., Head, M. K., and Buenfeld, N. R., (2006). "Pore segmentation of cement-based materials from backscattered electron images." *Cement and Concrete Research,* 36(6), 1083-1090.

Xiao, J. Z., Li, W. G., Sun, Z. H., Lange, D. A., and Shah, S. P., (2013). "Properties of interfacial transition zones in recycled aggregate concrete tested by nanoindentation." *Cement and Concrete Research,* 37, 276-292.

Ye, G., (2003). "*Experimental study and numerical simulation of the development of the microstructure and permeability of cementitious materials.*" PhD. thesis, Delft University of Technology, The Netherlands.

Zhang, J., and Scherer, G. W., (2011). "Comparison of methods for arresting hydration of cement." *Cement and Concrete Research,* 41(10), 1024-1036.

Zhang, P., Li, S. X., and Zhang, Z. F., (2011). "General relationship between strength and hardness." *Materials Science and Engineering, A* 529, 62-73.

Zhou, J., (2006). "*Microstructure and Permeability of Portland cement bleded with Blast furnace slag, Fly ash and Limestone powder.*" MSc. thesis, Delft University of Technology, The Netherlands.

Zhou, J., (2010). "*Performance of engineered cementitious composites for concrete repairs*." PhD. Thesis, Delft University of Technology, The Netherlands.

Zhu, W. and Bartos, P., (1997). "Assessment of interfacial microstructure and bond properties in aged GRC using a novel microindentation method." *Cement and Concrete Research,* 27(11), 1701-1711.